Dissociation dynamics of the methylsulfonyl radical and its photolytic precursor CH_3SO_2Cl

Bridget W. Alligood,[1] Benjamin L. FitzPatrick,[1] Emily Jane Glassman,[1] Laurie J. Butler,[1,a)] and Kai-Chung Lau[2,a)]
[1]*Department of Chemistry and The James Franck Institute, University of Chicago, Chicago, Illinois 60637, USA*
[2]*Department of Biology and Chemistry, City University of Hong Kong, Hong Kong*

(Received 11 November 2008; accepted 19 March 2009; published online 22 July 2009)

The dissociation dynamics of methylsulfonyl radicals generated from the photodissociation of CH_3SO_2Cl at 193 nm is investigated by measuring product velocities in a crossed laser-molecular beam scattering apparatus. The data evidence three primary photodissociation channels of the precursor: S–Cl fission to produce Cl atoms and ground electronic state CH_3SO_2 radicals, S–Cl fission to produce Cl atoms and electronically excited CH_3SO_2 radicals, and $S-CH_3$ fission. Some of the vibrationally excited CH_3SO_2 radicals undergo subsequent dissociation to CH_3+SO_2, as do all of the electronically excited radicals. The velocities of the SO_2 products show that the vibrationally excited ground state CH_3SO_2 radicals dissociate via a loose transition state having a small exit barrier beyond the endoergicity. Hence, a statistical recoil kinetic energy distribution should and does fit the distribution of velocities imparted to these SO_2 products. The electronically excited CH_3SO_2 radicals also dissociate to CH_3+SO_2, but with a larger average release to relative kinetic energy. Interestingly, when using 200 eV electron bombardment detection, the ground electronic state CH_3SO_2 radicals having too little internal energy to dissociate are not observed at the parent $CH_3SO_2^+$ ion, but only at the CH_3^+ daughter ion. They are distinguished by virtue of the velocity imparted in the original photolytic step; the detected velocities of the stable radicals are consistent with the calculated barrier of 14.6 kcal/mol for the dissociation of CH_3SO_2 to CH_3+SO_2. We present CCSD(T) calculations of the adiabatic excitation energy to the lowest excited state of CH_3SO_2 radicals, the 1 $^2A''$ state, as well as the vertical energy from the equilibrium geometry of that excited state to the 2 $^2A''$ state, to aid in the experimental assignment. © *2009 American Institute of Physics*. [DOI: 10.1063/1.3159555]

I. INTRODUCTION

Sulfur-containing radicals in the troposphere play a dynamic role in the oxidation of dimethyl sulfide (DMS) to sulfur dioxide (SO_2). The formation of SO_2 and its subsequent conversion into the sulfate anion (SO_4^{2-}) is of significant environmental concern due to the latter's role in acid rain and its effect on global climate. While the major anthropogenic source of SO_2 is the combustion of sulfur-containing fossil fuels, the major natural sources of SO_2 in the troposphere are from volcanic injection and the atmospheric oxidation of both DMS and carbon disulfide (CS_2).[1] Among these natural sources, DMS—emitted by ocean phytoplankton—is the largest contributor of SO_2. Investigating the reaction dynamics of the radical species involved in DMS oxidation may lead to an enhanced understanding of branching to stable end products. Specifically, the temperature dependence of this branching, as displayed in models of atmospheric oxidation of DMS, can perhaps be better understood by considering the competition between both the rates of formation and dissociation of various adducts and the reactions of these adducts with other atmospheric species in the overall oxidation mechanism.[2,3] Two possible adducts formed in collisions of methyl radicals and SO_2 are methylsulfonyl (CH_3SO_2) and methoxysulfinyl (CH_3OSO).[3] The methylsulfonyl radical is the primary focus of this paper.

Sulfur-containing radicals present a challenge for benchmarking current electronic structure methods, both in predicting the energetics of such species and in predicting the barrier heights of their reaction pathways. Previously published theoretical work pertaining to the CH_3SO_2 system highlights the need for concrete experimental data regarding the energetics along the dominant reaction channels.[4–6] Table I gives the barrier heights for the dissociation of CH_3SO_2 to CH_3+SO_2, as calculated at various levels of theory. Zhu and Bozzelli[5] compared their computational results and concluded that, while G3 methods gave good energetics, the CCSD(T) method was unreliable. Even though this latter conclusion was flawed, as the small basis size was not taken into account, it does illustrate the challenge in arriving at good predictions for these sulfur-containing molecules and the need for reliable experimental benchmarks. The preceding paper presents a basis set convergence analysis[7] showing that good energetics for the dissociation barrier to CH_3+SO_2 are obtained with the CCSD(T) method if one includes not only inner polarization functions (tight-*d* functions) in

a)Authors to whom correspondence should be addressed. Electronic address: L-Butler@uchicago.edu and kaichung@cityu.edu.hk.

TABLE I. Barrier heights for the dissociation of CH_3SO_2 to CH_3+SO_2, as calculated at various levels of theory. The large range of values highlights the need for experimental benchmarks for this system.

Calculated barrier[a] (kcal/mol)	Electronic structure method
15.4 (298 K)	G3(MP2)[5]
17.7 (298 K)	CBS-QB3[5]
14.3 (0 K)	G2(MP2) (geometry optimized with UMP2(Full)/6-31+G(2d,p))[4]
14.9 (298 K)	B3LYP/6-311++G(d,p)[5]
9.9 (298 K)	CCSD(T)/6-311G(d,p) (geometry optimized with MP2/6-31G(d,p))[5]

[a]To compare 298 K to 0 K values, the 298 K barrier calculated at the G3//B3LYP/6-311++G(3*df*,2*p*) level is 0.8 kcal/mol higher than the 0 K value.

the basis functions for the sulfur atom, as suggested in seminal work by Martin,[8] but also core-valence and relativistic corrections.

Some prior studies have also attempted to elucidate the unimolecular dissociation dynamics of the other CH_3+SO_2 adduct, CH_3OSO. Frank and Turecek, in 1999, predicted that the CH_3OSO radical dissociates to CH_3+SO_2 solely through isomerization to CH_3SO_2. These results were obtained primarily from statistical from Rice–Ramsperger–Kassel–Marcus (RRKM) theory, based on a calculated isomerization barrier of 23.4 kcal/mol—approximately 10 kcal/mol lower than the barrier to direct dissociation of CH_3OSO to CH_3 and SO_2. In contrast, Zhu and Bozzelli's calculated barrier at the G3(MP2) level of theory suggested that CH_3OSO can dissociate directly without isomerization, having a barrier to direct dissociation approximately 20 kcal/mol lower than the isomerization barrier.

Previous efforts to experimentally measure the unimolecular dissociation rate of the CH_3SO_2 radical have also been made, again with inconsistent results. Le Bras and coworkers have tried to indirectly measure the unimolecular dissociation rate of the CH_3SO_2 radical via kinetic modeling in mixtures, leading to results that vary by more than an order of magnitude.[9–11] More recently, Baronavski and coworkers used time-resolved photoionization in an attempt to directly measure the unimolecular dissociation lifetime of the methylsulfonyl radical under collision-free conditions. Using methylsulfonyl chloride (CH_3SO_2Cl) as a photolytic precursor, their data[6] evidenced a time dependent decay of the signal at $m/e=79$, $CH_3SO_2^+$, with a lifetime of 0.34 ps; their data also showed a negligible ($<2\%$) fraction of the signal assigned to CH_3SO_2 radicals remained after 2 ps. Using statistical RRKM theory, they then tried to fit their data using the $CH_3SO_2 \rightarrow CH_3+SO_2$ transition state calculated by Frank and Turecek, but they had no independent measurement of the internal energy distribution of the dissociating radicals. To obtain a rate constant for CH_3SO_2 dissociation that was comparable to their measured rate, they had to assume an initial distribution of nascent radicals that peaked near 24 kcal/mol and extended below the dissociation barrier. While this estimated distribution effectively reproduced the measured dissociation rate, it did not successfully predict the fraction of undissociated radicals. The signal observed at $CH_3SO_2^+$ decayed to $<2\%$ after 2 ps, while the model predicted that about 13% of the nascent radicals would remain undissociated.

In attempting to resolve the problems noted above, the present work first directly determines the internal energy distribution of the nascent CH_3SO_2 radicals formed from the photodissociation of methylsulfonyl chloride at 193 nm; it then probes the subsequent unimolecular dissociation dynamics of these radicals. The data clearly show that, with the same photolytic precursor as used by Baronavski and coworkers, a significant fraction of the nascent CH_3SO_2 radicals are formed in an excited electronic state; furthermore, the data suggest that the dissociation of these electronically excited radicals does not occur via internal conversion to the ground electronic state. The data also resolve the unimolecular dissociation of the nascent ground state radicals to CH_3+SO_2 and show that a small fraction of CH_3SO_2 radicals remain undissociated due to their low internal energy. Thus, this work offers key data for validating emerging electronic structure calculations of these important radical intermediates.

II. METHODS

A. Experimental method

Our experiments allow us to produce CH_3SO_2 radicals under collision-free conditions and to characterize both their internal energy distribution and subsequent dynamics. We use a crossed laser-molecular beam apparatus to measure the distribution of velocities imparted to the Cl atoms, and thus their momentum-matched CH_3SO_2 radicals, that are produced from the photodissociation of a halogenated precursor, methylsulfonyl chloride (CH_3SO_2Cl). We then detect the nascent radicals formed with a low enough internal energy to be stable to subsequent dissociation, as well as the secondary dissociation products originating from the higher internal energy radicals. The molecular beam, composed of CH_3SO_2Cl seeded in He (details below), passes through two skimmers *en route* to the main chamber where it intersects the output of a pulsed excimer laser producing 193.3 nm. The propagation axis of the laser beam is perpendicular to the plane defined by the molecular beam and the line from this interaction region to the detector, so the excitation light is unpolarized in

the scattering plane. (For the angular distribution measurements described later, the polarization vector of the light is rotated in this plane.) The source region, containing the molecular beam nozzle, can be rotated to facilitate data collection at different source angles. Upon photodissociation, neutral dissociation products scatter from the interaction region with velocities determined by the vector sum of the molecular beam velocity and the recoil velocity imparted during the dissociation. Those scattering into the 1.5° acceptance angle of the differentially pumped detector travel 44.6 cm to an electron bombardment ionizer and are ionized by 200 eV electrons.[12] These ions are then accelerated and focused by high voltage lenses toward the entrance to a quadrupole mass spectrometer, where they are mass selected and detected using a Daly detector.[13] The resultant voltage pulses are counted by a multichannel scaler, giving a signal proportional to the number of ions at each mass-to-charge ratio as a function of time after the dissociating light pulse. The signal is accumulated in 2 μs channels; all data and fit points are plotted at the end of each time window. The signal comes from parent and daughter ions of both the neutral photofragments and the products formed from the dissociation of any unstable radicals. Upon subtraction of the calibrated ion flight time, calculated using the apparatus' measured ion flight constant of 4.5 μs amu$^{-1/2}$, forward convolution fitting of the time-of-flight (TOF) spectrum determines the distribution of energies imparted to relative product translation in the dissociation, E_T.

The molecular beam is formed by seeding the equilibrium vapor pressure of CH_3SO_2Cl at 20 °C in He gas, yielding a total stagnation pressure of 420 Torr, and expanding the mixture through a continuous (not pulsed) nozzle heated to 100 °C and having an orifice diameter of approximately 0.006 in. To characterize the parent beam, we rotate the source to point directly into the detector and raise a 300 Hz chopper wheel into the beam. The neutral flight path is determined similarly, but with a neat He beam and an unheated nozzle. The number density distribution of velocities in the molecular beam typically peaks at 1700 m/s, with a full width at half maximum of 11%. To measure the velocities of the neutral photofragments reported in this paper, the molecular beam source is rotated to different angles in the plane containing the beam and detector axis, which is perpendicular to the laser beam propagation direction. The angle at which data are acquired is indicated in the upper right corner of all presented spectra.

The 193 nm light is produced from the ArF transition of an unpolarized Lumonics PM-848 excimer laser. The laser is focused down to a beam spot with a ~6 mm^2 cross-sectional area in the interaction region. Over the course of the experiment, the laser powers range from 4 to 18 mJ/pulse; the exact power used for each spectrum is noted when relevant.

Beyond the data presented herein, we also looked for signal at $m/e=16$ (O^+), $m/e=29$ (CHO^+), $m/e=31$ (CH_3O^+), $m/e=32$ (O_2^+,S^+), $m/e=47$ (CH_3S^+,$CH_3O_2^+$,CCl^+), $m/e=66$ (CH_3OCl^+), $m/e=82$ (CH_3SCl^+,$CH_3O_2Cl^+$), $m/e=83$ ($SOCl^+$), $m/e=99$ (SO_2Cl^+), and $m/e=114$ ($CH_3SO_2Cl^+$). While at $m/e=29$, 31, 47, 66, 82, 83, 99, and 114, little or no significant signal appeared above the noise at the end of 3×10^6 laser shots, at $m/e=16$ and $m/e=32$ we did see 125 000 and 160 000 counts of integrated signal after 6×10^6 and 3×10^6 laser shots, respectively. We also observed significant signal at $m/e=48$, about 35 000 counts in 1×10^6 laser shots, and investigated the laser power dependence of that spectrum. We do not include fits to these data in Sec. III below as the multiple possible single and multiphoton contributions to these spectra prohibit making definitive conclusions regarding them; the respective time-of-flight spectra are shown in the EPAPS supplement.[14]

To measure the angular distribution of the recoiling Cl fragments, the unpolarized laser pulses at 193.3 nm were separated into two linearly polarized beams with a Spectra Physics single-crystal quartz birefringent Pellin–Broca prism. The polarization vector of the light was changed by passing the horizontally polarized component through a half-wave retarder. Before the experiments, the purity of the light's polarization and the orientation of the optic axis of the half-wave retarder were verified using a second birefringent Pellin–Broca prism. The polarized light, with pulse energy of about 4 mJ, was focused to a ~2 mm^2 spot at the interaction region. Looking in the direction of propagation of the light, the polarization angles are rotated clockwise from the detector axis while the molecular beam source angle was set to 30° counterclockwise from that axis. Data were collected at $m/e=35$ for seven polarization angles; a total of 8×10^5 shots were taken at each angle, split into four sets of 2×10^5 each. The measurement order of different angles was permuted between data collection sets in order to average out drifts in molecular beam and laser intensities over time. The angular distribution of the Cl fragments was determined by integrating the time-of-flight distribution of the recoiling Cl fragments over the relevant time frame.

B. Computational methods

Although the preceding paper presents state-of-the-art electronic structure calculations at the CCSD(T) level of theory, we recalculated the minima and transition states relevant to the CH_3SO_2 system here with the modified G3//B3LYP method[15] using the GAUSSIAN03 electronic structure package.[16] This less computationally expensive method is commonly used when studying larger systems and includes a recent reparameterization for third row atoms, so the comparison helps validate the method. Our calculations also revealed some errors in prior computational results on this system. We optimize the geometries of each minimum and transition state using the B3LYP method with a 6-311++G($3df$,$2p$) basis set and a spin-unrestricted reference. The basis set is chosen by adding diffuse and polarization functions to 6-311$G(d,p)$ until a consistent geometry is achieved. The geometries are converged to a root-mean-square (rms) force below 1×10^{-5} and a rms displacement below 4×10^{-5}, where both are in atomic units. Intrinsic-reaction-coordinate (IRC) calculations are also performed at the B3LYP/6-311++G($3df$,$2p$) level of theory for each transition state to assure each corresponds to the correct reactants

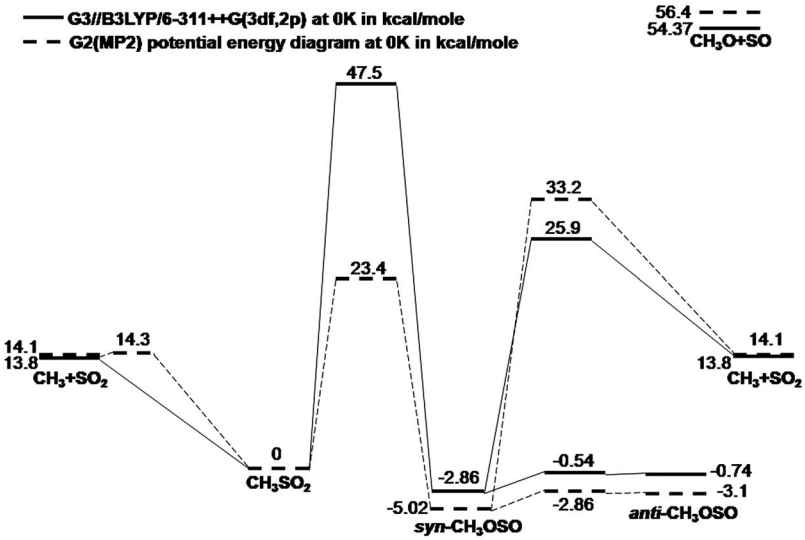

FIG. 1. The dashed lines show the critical points on the potential energy surface as published by Frank and Turecek at the G2(MP2) level of theory, using geometries optimized at UMP2(full) with a 6-31+G($2d,p$) basis set. The solid black lines represent the critical points on the potential energy surface we calculated with G3//B3LYP/6-311++G($3df,2p$). The barrier height for the isomerization between the *syn*-CH_3OSO and CH_3SO_2 radicals differs by about 24 kcal/mole in going from G2(MP2) to G3//B3LYP; further investigation shows that Frank and Turecek were reporting a spurious transition state altogether.

and products. All of the relevant structures, moments of inertia, and harmonic vibrational frequencies are given in the supplementary EPAPS document.

The vertical excitation energies, from the ground state equilibrium structure to the excited CH_3SO_2 ($^2A'$ and $^2A''$) states, are predicted using the equation-of-motion coupled cluster method (EOMEE−CCSD) implemented in the ACESII software.[17] A few excited-state energies of the higher $^2A''$ states are computed at the equilibrium geometry of the 1 $^2A''$ excited state of CH_3SO_2 in efforts to set an upper bound for the adiabatic excitation energy to those states. Both the ground state structure and the first excited-state structure of CH_3SO_2 are optimized at the CCSD(T)/6-311++G($2df,p$) level of theory. Zero-point vibrational energy correction is not included in the vertical excitation energies. The adiabatic excitation energy of the first excited $^2A''$ state is calculated at the CCSD(T)/aug-cc-pV(Q+d)Z//CCSD(T)/6-311++G($2df,p$) level of theory using restricted open-shell Hartree–Fock based coupled cluster theory with single and double excitations plus perturbative triple excitations [ROHF-UCCSD(T)] with the MOLPRO package.[18] The adiabatic excitation energy includes the zero-point energy correction and scalar-relativistic and core-valence correlation effects (refer to preceding paper for details).

III. RESULTS AND ANALYSIS

A. Computational results on CH_3SO_2 radicals and comparisons with prior work

To begin our work on this system, we recalculated a portion of the minima and transition states on the CH_3SO_2 potential energy surface at the G3//B3LYP/6-311++G($3df,2p$) level of theory and investigated the discrepancies when comparing with prior computational results on this system. Our results, shown in Fig. 1, differ from the CCSD(T) results (see the preceding paper) in every instance by no more than 2.5 kcal/mol, giving some confidence to using the less computationally expensive method for a crude prediction of the relevant energetics. Our calculations also give results similar to those published by Zhu and Bozzelli at the G3(MP2) level of theory. In comparing with Frank and Turecek's surface, however, we noted a significant disagreement in the transition state for isomerization of CH_3SO_2 to CH_3OSO, reported as a 23.4 kcal/mol barrier by Frank and Turecek and determined to be 47.5 kcal/mol in our G3//B3LYP calculations. While Frank and Turecek did use the earlier G2(MP2) method, with geometries optimized at the UMP2(full)/6-31+G($2d,p$) level of theory, it was nevertheless surprising that the G2(MP2) method would give such a dramatically lower isomerization barrier than the G3//B3LYP method. To investigate the difference, we first recalculated our transition state structure and energy, as originally calculated with G3//B3LYP, at the G2(MP2) level of theory used by Frank and Turecek in an attempt to reproduce their results; the resulting barrier was 49.7 kcal/mol, suggesting that the 23.4 kcal/mol barrier reported by Frank and Turecek was not the transition state along the isomerization reaction coordinate. The corrected G2(MP2) results are given in the EPAPS supplement. We then performed IRC calculations on both our transition state structure as well as the structure reported by Frank and Turecek. Our IRC calculations show that Frank and Turecek were probably observing a spurious transition state altogether.

As the experimental data given in the subsequent sections of this paper evidenced electronically excited CH_3SO_2 radicals, we analyzed the molecular orbitals and the electronic configurations of the ground and the low-lying excited states of the CH_3SO_2 radical. The ground state has $^2A'$ symmetry with the radical electron in a nonbonding a' orbital localized on the S atom. The first electronically excited state has $^2A''$ symmetry; its dominant configuration in the Franck–Condon region is best described by excitation of an electron from a nonbonding a'' orbital on one of the O atoms to the a' orbital on the S atom that was singly occupied in the ground state configuration. The vertical excitation energies for various $^2A'$ and $^2A''$ excited states of CH_3SO_2 are summarized in Table II. We also optimized the geometry while enforcing the 1 $^2A''$ symmetry to calculate the adiabatic excitation energy from the ground state to the zero-point level in the lowest excited state. That value, 34.8 kcal/mol, compares favorably

TABLE II. Calculations of the electronically excited states of the CH_3SO_2 radical. All energies are in kcal/mol.

Electronic state	Vertical excitation energies[a]	Adiabatic excitation energies
$\tilde{X}^2A'$	0	
$1\ ^2A''$	75.2	34.8[b]
$2\ ^2A''$	83.7	<45.5 [c]
$2\ ^2A'$	85.8	
$3\ ^2A'$	147.0	
$4\ ^2A'$	152.3	
$3\ ^2A''$	161.6	

[a]Calculated with the EOMEE-CCSD/cc-pVTZ method; the zero of energy is taken as the minimum of the ground electronic state.
[b]Based on the single-point energy calculations at the CCSD(T)/aug-cc-pV(Q+d)Z//CCSD(T)/6-311++G(2*df*,*p*) level. The excitation energy includes zero-point energy correction as well as scalar-relativistic and core-valence correlation effects, which are detailed in the preceding paper. For this number, the zero of potential energy is set at the zero-point vibrational level in the ground electronic state.
[c]We estimate this upper limit to the adiabatic excitation energy from the difference between the $1\ ^2A''$ (32.2 kcal/mol) and $2\ ^2A''$ (42.9 kcal/mol) states (at the equilibrium geometry of the $1\ ^2A''$ state), calculated at the level of theory described in footnote "a", and add this difference to the adiabatic excitation energies of $1\ ^2A''$ (34.8 kcal/mol).

to the rough onset of the S–Cl fission channel assigned to the formation of excited-state radicals in the experiments below.

B. S–Cl bond fission and the internal energy distribution of the nascent CH_3SO_2 radicals

Figure 2 shows the time-of-flight spectra taken at $m/e=35$. Most of the signal in these spectra is Cl atoms resulting from primary S–Cl bond photofission in CH_3SO_2Cl. Forward convolution fitting of the signal taken with a 30° source angle is used to derive the S–Cl bond fission recoil kinetic energy distribution, $P(E_T)$, shown in solid gray line in Fig. 3. Fitting the signal with flight times between 100 and 150 μs gives the high kinetic energy portion, shown in long-dashed line in Fig. 3. This portion of the S–Cl bond fission $P(E_T)$, extending from near 30 to 80 kcal/mol, corresponds to high velocity, low internal energy CH_3SO_2 radicals whose internal energy distribution spans the theoretically predicted barrier for dissociation to CH_3+SO_2. At intermediate flight times, the signal in the Cl^+ spectrum peaks again, near 180 μs, indicating a second dynamical pathway that produces $Cl+CH_3SO_2$. We assign this to the formation of radicals in one or both low-lying excited states, the $1\ ^2A''$ and $2\ ^2A''$ states of CH_3SO_2. This assignment is supported by the observed dissociation dynamics of these radicals reported in Secs. III C and III D. The $P(E_T)$ for formation of Cl atoms and excited-state CH_3SO_2 radicals is derived from the forward convolution fit to this intermediate signal, shown by the short-dashed line; it extends from 0 to about 50 kcal/mol in recoil kinetic energy. The lowest lying excited state, as delineated in Sec. III A, was calculated to have an adiabatic excitation energy of 34.8 kcal/mol; it is, therefore, energetically allowed across the entire component of the S–Cl bond fission $P(E_T)$ shown in short-dashed line in Fig. 3. The spectrum taken with a 10° source angle shows an additional signal peaking near 300 μs, which—accounting for small differences in ion flight times—appears in the $CH_3SO_2Cl^+$, Cl^+, $CH_3SO_2^+$, CH_3^+, SO^+, O_2^+, and SO_2^+ data; this signal is attributed to the dissociation of molecular clusters ($(CH_3SO_2Cl)_n$) in the beam. That component is derived from forward convolution fitting of the signal in the $CH_3SO_2^+$ spectrum taken under similar beam conditions (see Fig. 5 for an example), where it is not overlapped by any other signal; the resulting velocity distribution of this signal is used to fit the cluster contribution in all spectra in this paper. It is shown in dash-dot-dashed line in Fig. 2 and 5–7.

For those S–Cl bond fission events partitioning the highest relative kinetic energy to the recoiling Cl atoms, the momentum-matched CH_3SO_2 radicals are formed with low internal energies, some below the predicted barrier for the radicals to dissociate to CH_3+SO_2. Section III C shows that the stable radicals do not give signal at parent ion upon electron bombardment ionization, but instead give signal at the CH_3^+ daughter ion. The internal energy distribution of all nascent radicals, both stable and unstable, is determined from energy conservation using the total recoil kinetic energy distribution shown in Fig. 3, as derived from the measured Cl atom velocities and momentum conservation. For each measured recoil kinetic energy E_T, we calculate the internal energy in a nascent CH_3SO_2 radical from,

$$E_{\text{int}}(CH_3SO_2) = h\nu + E_{\text{parent}} - D_0(S-Cl) - E_{Cl} - E_T. \quad (1)$$

Here the CCSD(T) value of 65.6 kcal/mol (from the preceding paper) is used for the dissociation energy of the S–Cl bond, D_0. It is close to the G3//B3LYP/6-311++G(3*df*,2*p*) value of 66.5 kcal/mol. The photon energy $h\nu$ is 147.8 kcal/mol, and the energy in spin-orbit excitation of the Cl atom product is denoted E_{Cl}. E_{parent} is estimated by assuming that the rotational energy of the CH_3SO_2Cl molecules is effectively cooled in the supersonic expansion, but that the vibrational energy is characterized by the average of a thermal distribution at the nozzle temperature. This is calculated to be 2.8 kcal/mol using unscaled CCSD(T) frequencies obtained with a 6-311++G(2*df*,*p*) basis set. E_{Cl} is 0 kcal/mol for CH_3SO_2 radicals produced in conjunction with ground state $Cl(^2P_{3/2})$ atoms and 2.5 kcal/mol for radicals produced in conjunction with spin-orbit excited-state $Cl(^2P_{1/2})$ atoms. In the preceding paper, we are able to separately determine the kinetic energy distributions resulting in each spin-orbit state using REMPI detection of the Cl atoms; for simplicity, we include this small additional internal energy with that of the radicals for the plots in this paper.

Figure 4 shows the derived internal energy distribution of the CH_3SO_2 radicals superimposed on the relevant portion of the potential energy surface. One would expect any CH_3SO_2 radicals formed with an internal energy below the CCSD(T) predicted barrier at 14.6 kcal/mol, shown in thin-dashed line, to be stable; at internal energies above this line, however, radicals may be stable if some of the overall internal energy were partitioned into rotation rather than vibration of the CH_3SO_2 radical or to spin-orbit excitation of the Cl cofragment. Thus, to aid us in predicting where we might see signal from stable radicals, we also superimpose on this figure the results from the preceding paper. In those imaging experiments, we detect stable radicals using 10.5 eV photo-

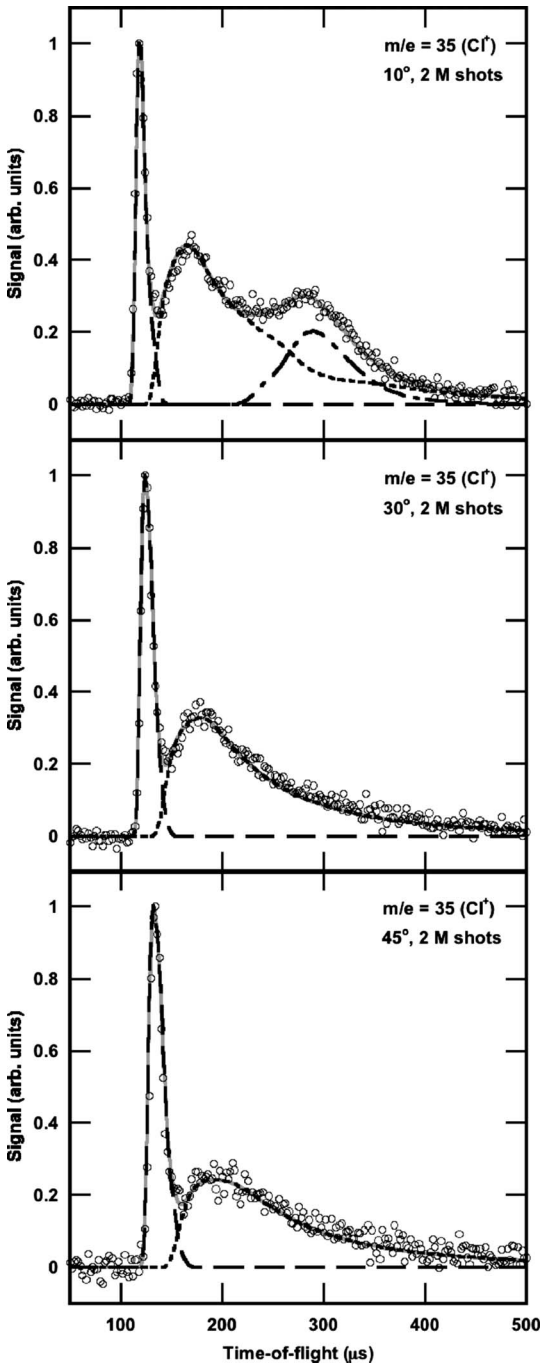

FIG. 2. TOF spectra at $m/e=35$ (Cl^+) from the photodissociation of methylsulfonyl chloride using unpolarized light from the excimer. The three frames shown here are from data acquisition at 10°, 30°, and 45° (from top frame to bottom frame). The data are shown in open circles, and the total forward convolution fit to the data (shown in gray solid line) is the sum of three contributions, shown here in long-dashed, short-dashed, and dash-dot-dashed lines. The contributions from Cl atoms formed in the photodissociation of methylsulfonyl chloride, shown in long-dashed line and short-dashed line, are calculated from the corresponding portions of the total recoil translational energy distribution in Fig. 3. The short-dashed line fits the signal assigned to $CH_3SO_2Cl+h\nu \rightarrow$electronically excited CH_3SO_2 ($1\ ^2A'', 2\ ^2A''$) +Cl. The longer-dashed line fits the signal assigned to $CH_3SO_2Cl+h\nu \rightarrow CH_3SO_2$ ($\tilde{X}\ ^2A'$)+Cl. The top spectrum also includes a contribution (dash-dot-dashed line) from the photodissociation of clusters in the molecular beam; the spectator CH_3SO_2Cl dissociatively ionizes to Cl^+. This fit is determined from the signal in Fig. 5. The measurement order of the data obtained at different source angles was permuted between data collection sets in order to average out drifts in molecular beam and laser intensity over time. We note a small but systematic error in the fits; the fast edge is underfit at smaller source angles and overfit at larger angles.

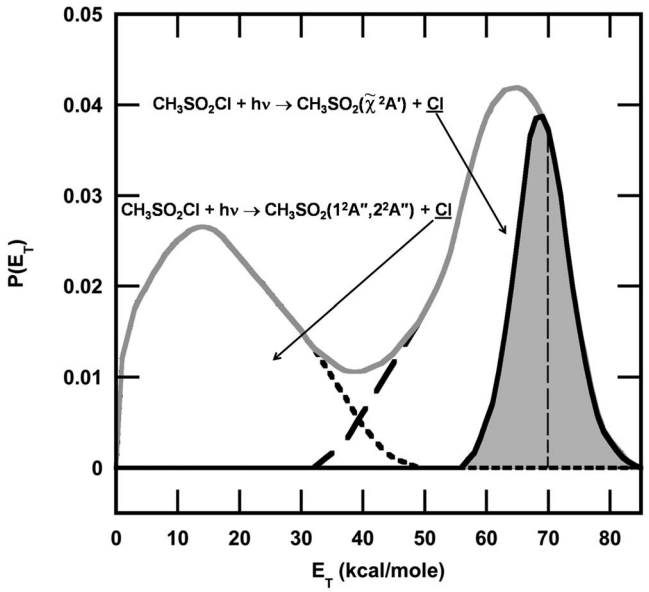

FIG. 3. The total recoil kinetic energy distribution for the S–Cl bond fission in methylsulfonyl chloride photodissociating at 193 nm. This distribution was derived from forward convolution fitting of the Cl atom TOF spectrum shown in the middle frame of Fig. 2, with the assumption that the angular distribution of S–Cl fission photofragments is constant as a function of recoil kinetic energy. The solid gray line is the overall fit obtained; the dashed lines show the same fit, but approximately separated into two components. The shaded region shows the stable CH_3SO_2 radicals, as obtained in the imaging experiments, and shifted to 1 kcal/mol higher translational energies. The thin, black dashed line illustrates the sharply truncated kinetic energy threshold calculated from the theoretical barrier using Eq. (1) and assuming all the internal energy in the CH_3SO_2 radicals is partitioned to vibration of the radicals, not rotation; this truncation point would shift to lower kinetic energies by 2.5 kcal/mol for CH_3SO_2 radicals formed in conjunction with $Cl(^2P_{1/2})$.

ionization [see Fig. S.8 and the solid line in Fig. S.9 from the supporting documents for the preceding paper; these figures show the image and the $P(E_T)$ for these stable radicals]; that distribution of radicals is shown in the shaded portion in Fig. 4. Figure 4 also shows the calculated adiabatic excitation energy to the lowest excited state, the $1\ ^2A''$ state, of CH_3SO_2. The next higher excited state, the $2\ ^2A''$ state, is also energetically allowed for most of the higher internal energy radicals. We return to this in the analysis of the dissociation dynamics of the CH_3SO_2 ground and excited-state radicals below. Figure 4 shows that a significant fraction of the nascent ground state CH_3SO_2 radicals from the high-recoil kinetic energy S–Cl bond fission channel have an internal energy below that required to dissociate to CH_3SO_2. The next section describes our search for signal from those stable radicals.

We note that the relative weightings of the two channels shown in Figs. 3 and 4 were obtained by analyzing data from an unpolarized laser and assuming the angular distributions of the Cl atoms from the components of the $P(E_T)$ are the same. However, the data presented in Sec. III F below show that the angular distributions of the Cl fragments in the high and low kinetic energy portions of the $P(E_T)$ have somewhat different anisotropy parameters β. Even with an unpolarized laser, one must correct the observed intensities of the signal from each channel by a factor of $(1+\beta/4)^{-1}$ to account for

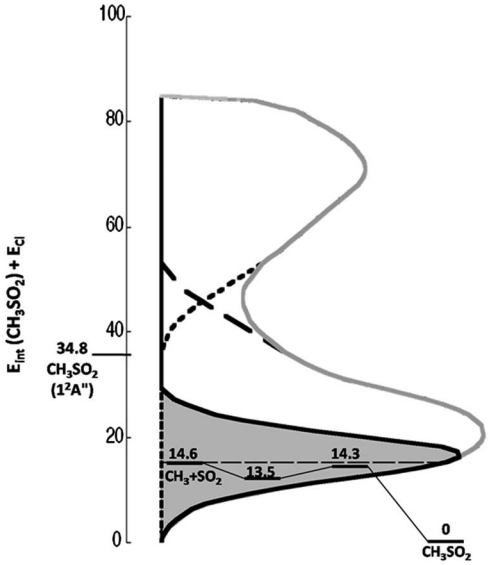

FIG. 4. The internal energy distribution of the methylsulfonyl radicals from S–Cl bond fission in methylsulfonyl chloride as derived from the measured total recoil kinetic energy distribution in Fig. 3 and using conservation of energy as given by Eq. (1). The distribution is superimposed on the zero-point corrected energetics for the $CH_3SO_2 \rightarrow CH_3+SO_2$ dissociation calculated at CCSD(T)/aug-cc-pV(Q+d)Z+ZPVE+core-valence+relativistic effects. The figure also shows the calculated adiabatic excitation energy to the $1\ ^2A''$ excited state of CH_3SO_2. The internal energy distribution of the nascent CH_3SO_2 radical extends well below the 14.6 kcal/mol barrier height, suggesting that we should be able to detect the presence of stable CH_3SO_2 radicals; the shaded region shows where these stable radicals were detected in the preceding paper. The bimodal nature of the distribution, along with the calculation of the first and second electronically excited states, suggests that we are forming radicals in both their ground and electronically excited states.

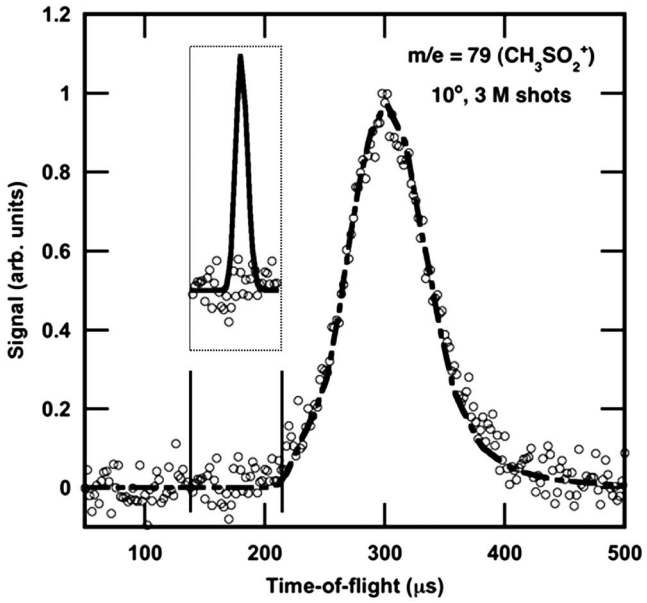

FIG. 5. TOF spectrum of the signal detected at $m/e=79$ ($CH_3SO_2^+$). The data are shown in open circles, and the dash-dot-dashed line is the forward convolution fit of the data. There is no signal in the spectrum at the flight time expected for stable CH_3SO_2, in the range of 180–200 μs; the area between the sharp, solid lines in the inset shows where these stable $CHSO_2$ radicals would appear. The broad signal extending from 210–410 μs is attributed instead to the photofragmentation of clusters in the molecular beam, when the spectator CH_3SO_2Cl is dissociated to $CH_3SO_2^+$. The fit for this signal, as it is presumably entirely from clusters, allows us to characterize cluster contributions in data obtained at all other masses (shown as dash-dot-dashed lines in Fig. 2, 6, and 7).

the fact that photofragments with a parallel angular distribution are more likely to be scattered in the detector plane. Thus, the relative weightings of the high kinetic energy to the low kinetic energy portion are adjusted from 1:0.76, to 1:0.72 when we account for the different anisotropy parameter characteristics of each channel.

C. Detecting the stable CH_3SO_2 radicals

Only the CH_3SO_2 radicals that are momentum matched to the highest velocity Cl atoms are formed with low enough internal energies to exist below the dissociation barrier depicted in Fig. 4. Thus, using the CCSD(T) calculated barrier of 14.6 kcal/mol, we can use the fastest Cl atom velocities to predict the velocity spectrum and TOF spectrum of the stable CH_3SO_2 radicals. This prediction, a sharp distribution peaking between 180 and 200 μs, is shown in the inset of Fig. 5 with a solid black line superimposed on the TOF signal detected at $m/e=79$, $CH_3SO_2^+$. There is no signal in that region of the TOF spectrum; clearly these radicals do not give significant parent ion upon 200 eV electron impact ionization, although they are detected at parent ion in the preceding paper upon photoionization at 10.5 eV. The broad, slow signal in the $m/e=79$ spectrum, which peaks near 300 μs, also appears in the $CH_3SO_2Cl^+$, Cl^+, $CH_3SO_2^+$, CH_3^+, SO_2^+, O_2^+, and SO^+ data; it is, therefore, easily assigned to the spectator monomer in the photodissociation of molecular clusters in the beam. Indeed, we fit this cluster signal in all of these spectra using the speed distribution determined from forward convolution fitting of the signal in the $m/e=79$ spectrum in Fig. 5 and correcting for the small difference in ion flight time through the mass spectrometer for each daughter ion of CH_3SO_2Cl. The cluster fit is shown in dash-dot-dashed line in each spectrum.

The $m/e=15$, CH_3^+, TOF spectrum in Fig. 6 is the only one displaying the sharp high-recoil velocity distribution expected for the component of the CH_3SO_2 radicals that are formed with an internal energy below the barrier to dissociation. The component of the fit, shown in a solid black line, retains only those CH_3SO_2 radicals that are formed in conjunction with the fastest Cl atoms; these are stable CH_3SO_2 radicals, and they dissociatively ionize to CH_3^+ daughter ions upon 200 eV electron bombardment ionization. The other fits in that spectrum show the contribution from cluster dissociation discussed previously, along with methyl radicals from three sources: the secondary dissociation of the higher internal energy ground state radicals, the methyl radicals from the dissociation of the electronically excited CH_3SO_2 radicals, and a contribution from very high kinetic energy methyl radicals that must come from another primary fission channel in the photodissociation of CH_3SO_2Cl, photocleavage of the $S-CH_3$ bond (discussed in Sec. III E). In the top frame of Fig. 6, the contributions of all three sources of methyl radicals are combined in the gray, dotted-line fit predicted from the velocity distribution of signal at $m/e=15$ detected with 10.5 eV photoionization (given in the preceding paper). Thus, in the top frame of Fig. 6, one can clearly identify the

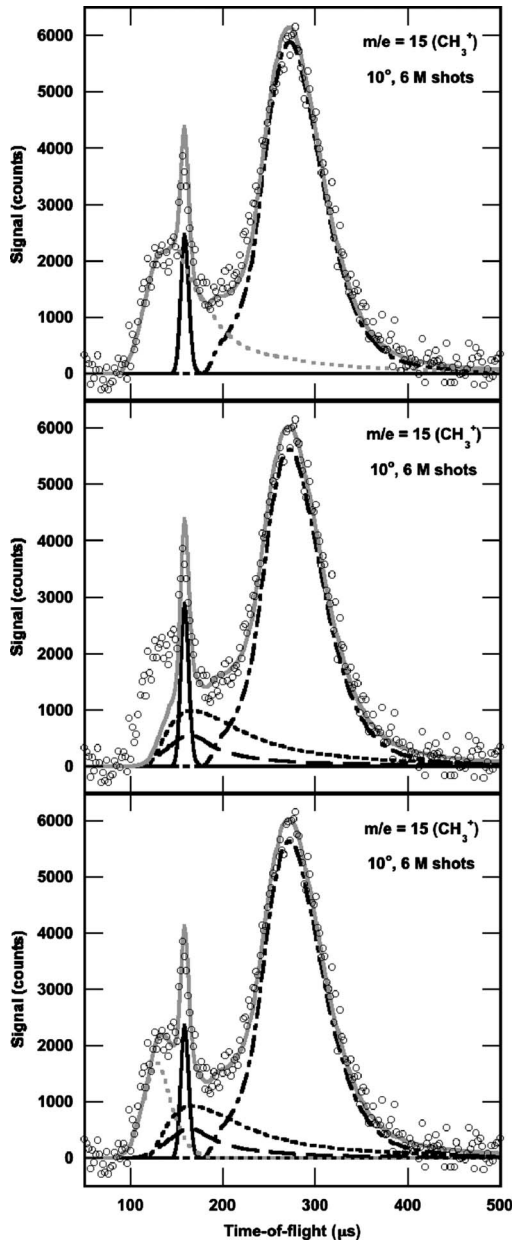

FIG. 6. TOF spectrum of the products detected at $m/e=15$ (CH_3^+). Open circles show the experimental data. In all spectra, the contribution from dissociative ionization of energetically stable CH_3SO_2 radicals is shown by the solid black line and is calculated from the shaded portion of the $P(E_T)$ in Fig. 3. These radicals are produced from high-recoil kinetic energy S–Cl fission events that leave the radicals with too little vibrational energy to surmount the barrier to unimolecularly dissociate to CH_3+SO_2. The solid gray line gives the overall fit. The dash-dot-dashed line shows the contribution from clusters discussed previously. In the upper frame we show that all of the remaining signal is well fitted by the speed distribution of the methyl radicals detected using 10.5 eV photoionization in the preceding imaging paper, shown in dotted gray line. The middle and lower frames identify the origin of these methyl radicals. In the middle spectrum, the only sources of methyl radicals shown are the short-dashed line corresponding to the methyl radicals from the secondary dissociation of the electronically excited CH_3SO_2 ($^2A''$), and the long-dashed line corresponding to the methyl radicals from the unimolecular dissociation of the ground electronic state CH_3SO_2 ($\tilde{X}\,^2A'$) as outlined in the text. Note that the fastest methyl radicals are unfit by these sources. The lower frame shows the contribution from very high kinetic energy methyl that must be due to another primary channel in the photodissociation of CH_3SO_2Cl, photocleavage of the $S-CH_3$ bond. It is calculated from the fast portion of the speed distribution of the methyl radicals detected from in the imaging experiment, again shown in dotted gray; the corresponding recoil kinetic energy distribution for $S-CH_3$ fission is shown in Fig. 10.

two additional contributions from dissociative electron impact detection, one from the dissociative ionization of stable radicals and one from clusters.

The excellent fit to the contribution in the $m/e=15$ spectrum from stable CH_3SO_2 radicals (which have dissociatively ionized to CH_3^+ upon electron impact ionization) is derived from the shaded portion of the $P(E_T)$ in Fig. 3. These are the stable radicals as detected at 10.5 eV in the imaging experiments and detailed in the preceding paper. We shift the entire distribution to 1 kcal/mol higher translational energies in order to account for the higher available energies resulting from our elevated nozzle temperature; this 1 kcal/mol of energy is justified by the difference in the E_{parent} at 100 °C (this experiment) and that at 25 °C (imaging experiment in preceding paper). In the supplemental document, we show a fit of the $m/e=15$ spectrum using only the rightmost portion of the shaded part of the $P(E_T)$ in Fig. 3—radicals formed from S–Cl bond fission events that partitioned more than 70 kcal/mol to translational energy. This is the portion that would leave the CH_3SO_2 radicals with less than 14.6 kcal/mol of internal energy, the CCSD(T) predicted barrier (assuming the Cl cofragment is in the ground spin-orbit state). Adequate fits to the spectrum could also be obtained by artificially moving the truncation point 3 kcal/mol higher or lower than this value. Hence, we did not refine our fitting to account for the fraction of radicals formed in conjunction with $Cl(^2P_{1/2})$ at each E_T. As the radicals are produced from the photodissociation of CH_3SO_2Cl, we do not expect much energy to be partitioned to rotational energy of the radicals, but clearly the fit to our data at $m/e=15$ is better if we account for the tail in the distribution of radicals measured in the imaging experiments. Further analysis of the distribution of radicals near threshold, which are stable by virtue of being formed in conjunction with $Cl(^2P_{1/2})$ or because they are formed with some energy in rotation rather than vibration, is included in the preceding paper.

D. SO_2 from the dissociation of ground state and electronically excited CH_3SO_2

The TOF spectrum obtained at $m/e=64$ (SO_2^+) and shown in Fig. 7 reveals the distinct dissociation dynamics of vibrationally excited ground state radicals as compared to the dissociation of electronically excited CH_3SO_2. As the unimolecular dissociation of the nascent ground-state CH_3SO_2 radicals occurs via a loose transition state with negligible barrier beyond the endoergicity, we expect the recoil kinetic energy distribution to be well represented by a statistical distribution at the transition state. To test this, we fit this component of the SO_2^+ signal; the fit is shown in long-dashed line in Fig. 7. The fit is obtained by the vector addition of the primary recoil velocity imparted to the ground electronic state CH_3SO_2 radicals [calculated from the portion of the S–Cl bond fission $P(E_T)$ shown in long-dashed line in Fig. 3, but excluding the shaded portion representing the CH_3SO_2 radicals below the unimolecular dissociation threshold] and the additional velocity of the SO_2 product as the vibrationally excited ground state radicals dissociate. The latter is

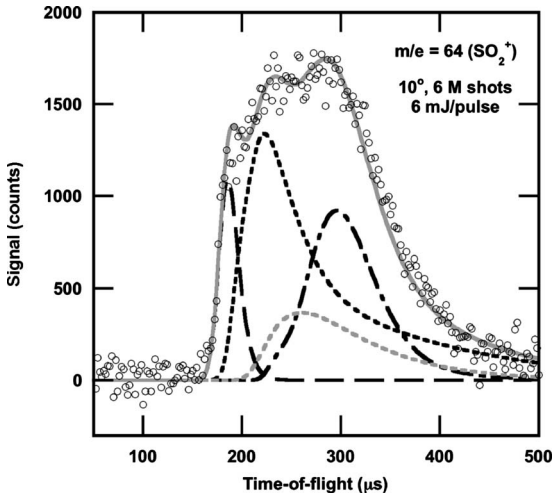

FIG. 7. TOF spectrum of the products detected at $m/e=64$ (SO_2^+) with laser energies of 6 mJ/pulse. The data are shown in open circles. The fit shown in long-dashed line reveals the contribution from dissociation products of the ground state radicals; the data are well fitted by the statistical secondary $P(E_T)$ shown in long-dashed line in Fig. 8. The contribution shown in dash-dot-dashed line is from clusters. The overall fit is given by the solid gray line. The short-dashed black line is from allowing only a portion of the excited-state radicals to dissociate (see Fig. 9). Figure S. 8 in the EPAPS document shows a spectrum obtained using higher laser power of 18 mJ/pulse; that spectrum could not be fitted with the entire distribution of electronically excited radicals, indicating that some of the excited-state radicals were being depleted before dissociating to CH_3+SO_2. Using the lower laser power, however, a significant portion of the excited-state radicals re-emerge; the fit of this data is shown by a short-dashed gray line. See Fig. 9 for the specific partitioning of the excited-state radicals used to fit these spectra. The secondary recoil kinetic energy distributions used to fit the SO_2 products from the dissociation of electronically excited radicals in this spectrum are shown in the corresponding short-dashed gray and black distributions in Fig. 8.

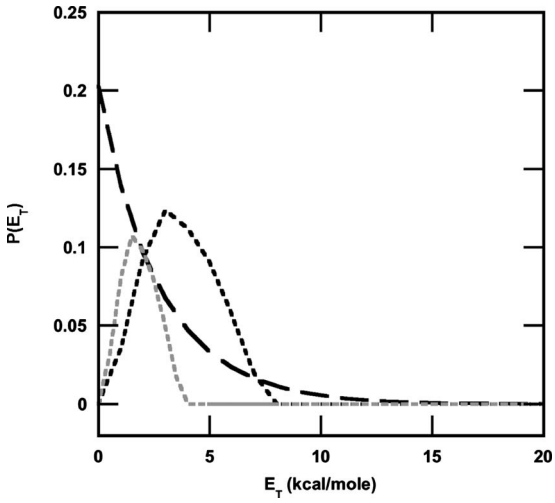

FIG. 8. The distribution of recoil kinetic energies imparted in the dissociation of ground state (long-dashed line) and excited-state (short-dashed line) CH_3SO_2 radicals to produce CH_3+SO_2. They are derived from fitting specific components of the signal at $m/e=64$ (SO_2^+) in Fig. 7 as described in the text. The dissociation of the ground state CH_3SO_2 radicals was well fitted by a statistical distribution, shown here in a long-dashed line. This figure explicitly shows how the two portions of the excited-state CH_3SO_2 were considered in fitting the lower power SO_2 signal shown in Fig. 7. The portions of the overall primary $P(E_T)$ considered are given in Fig. 9.

calculated from the statistical distribution shown in Fig. 8 in long-dashed line, obtained from RRKM theory using the CCSD(T) transition state and vibrational frequencies given in the preceding paper. The statistical prediction fits the observed recoil kinetic energies of these SO_2 radicals well.

In contrast, the SO_2 signal from the dissociation of electronically excited CH_3SO_2 radicals is not well fitted by a statistical recoil kinetic energy distribution. This is to be expected, as it is likely that excited electronic state radicals dissociate via electronic predissociation on an excited potential energy surface with a repulsive region at stretched C–S bond distances. This predissociation allows the partitioning to recoil kinetic energy between the CH_3 and SO_2 fragments to be much larger. To fit this contribution to the SO_2^+ spectrum, we first assumed that the entire distribution of electronically excited radicals produced from the short-dashed component of the S–Cl bond fission $P(E_T)$ shown in Fig. 3 dissociated to CH_3+SO_2 with a uniform distribution of recoil kinetic energies; these velocities are vector summed with various distributions for the subsequent dissociation to CH_3+SO_2. The recoil kinetic energy distribution for the dissociation, as determined from this forward convolution fitting procedure, is shown in the supplemental EPAPS document, along with the corresponding fit to the observed TOF distribution of SO_2 products. As expected, this kinetic energy distribution peaks well above 0 kcal/mol, reflecting the repulsive forces along the excited-state dissociation pathway; the signal appearing between 180 and 220 μs, however, was slightly underfit. Because there is no reason to expect that the highest internal energy excited-state radicals have quite the same dissociative behavior as those with lower internal energy, we attempted to fit the remaining signal using the divided $P(E_T)$ shown in Fig. 9 (details below). The excited-state radicals were treated in their entirety, but by allowing the portion under the dashed gray line to impart different recoil kinetic energies than the lower internal energy portion displayed by the dashed black line. The resulting fit and recoil translational energy distribution are shown in Figs. 7 and 8, respectively.

Data at $m/e=64$ (SO_2^+) were also taken at higher laser pulse energies—18 mJ/pulse as compared to the 6 mJ/pulse used in taking the data in Fig. 7. The data, shown in Fig. S.8 of the attached EPAPS supplement, suggest that CH_3SO_2 radicals formed in the lowest excited state, the $1\ ^2A''$ state, dissociate readily to form CH_3+SO_2, while radicals formed in one of the higher excited states, perhaps the $2\ ^2A''$ state, are, at the higher laser powers, selectively depleted by multiphoton excitation before dissociating.

We also obtained TOF spectra at $m/e=48$ (SO^+). The higher kinetic energy signal in this spectrum evidences a greater than linear dependence on laser power (see EPAPS supplement), resulting from the 193 nm photodissociation of some of the SO_2 products from the dissociation of CH_3SO_2 radicals. As the photodissociation of SO_2 at 193 nm is well understood, we did not attempt to further analyze this spectrum.

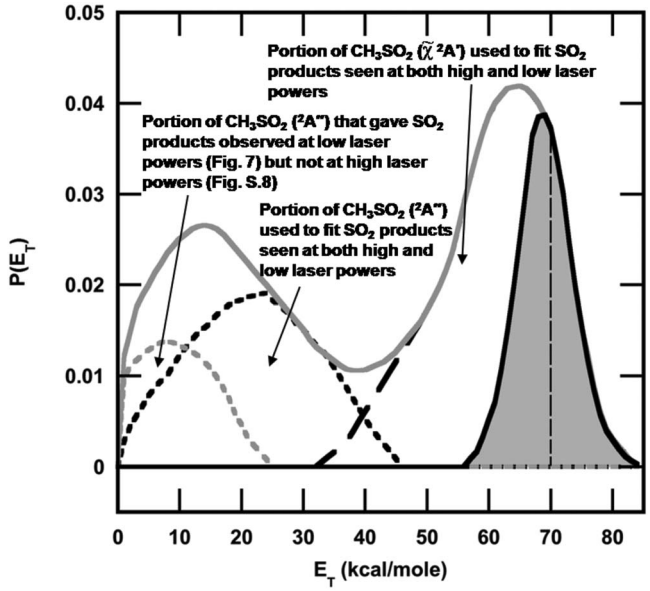

FIG. 9. The total recoil kinetic energy distribution for the S–Cl bond fission in methylsulfonyl chloride photodissociating at 193 nm. This distribution was derived from forward convolution fitting of the Cl atom TOF spectrum shown in the middle frame of Fig. 2. The solid line is the same fit as shown in Fig. 3. The long-dashed line corresponds to the ground state CH_3SO_2 radicals. The short-dashed lines are an arbitrary sectioning of the peak corresponding to the excited-state CH_3SO_2 radicals that gave a decent fit of the signal at $m/e=64$ (SO_2^+). The short-dashed gray portion, containing the slowest signal, is not considered in the secondary dissociation process at higher laser powers, as some of the CH_3SO_2 is preferentially depleted before dissociating.

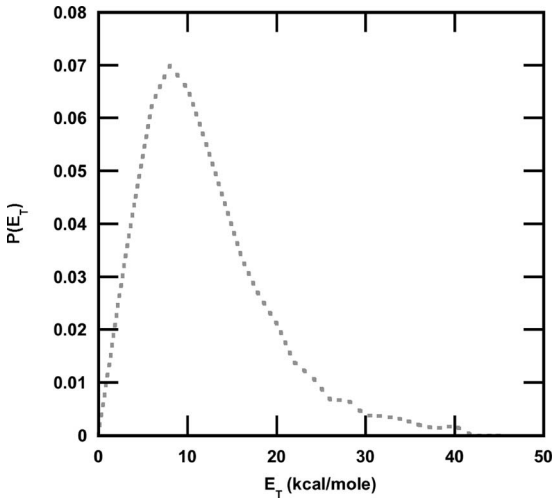

FIG. 10. The corresponding total recoil kinetic energy distribution for the primary S–CH_3 bond photofission channel used to fit the data in the lower frame of Fig. 6. Note that the true distribution of recoil kinetic energies is likely broader. This $P(E_T)$ is calculated from a portion of the imaging data in the preceding paper.

E. Evidence for an S–CH_3 bond fission channel in the photodissociation of CH_3SO_2Cl

In fitting the $m/e=15$ (CH_3^+) TOF spectrum in Fig. 6, we were unable to fit the signal at the earliest arrival times with the primary and secondary channels discussed so far. Although the entire signal is well fitted in the upper frame of Fig. 6, this fit is predicted from the velocity distribution $P(v)$ of the methyl radicals detected in the imaging experiment in our preceding paper. Some of these methyl radicals have too high of a velocity to arise from the dissociation of CH_3SO_2 radicals to CH_3+SO_2. For comparison, in the middle frame of Fig. 6, we show the shape of the components corresponding to methyl radicals from the dissociation of ground and excited electronic state CH_3SO_2 radicals using the same primary and secondary $P(E_T)$'s that fit the momentum-matched SO_2 signal in the higher power $m/e=64$ spectrum (in addition to the components from clusters and from dissociative ionization of the stable CH_3SO_2 radicals). The signal at the earliest arrival times is not accounted for by any of these sources and it did not evidence a multiphoton laser power dependence. Therefore, we assign this high velocity contribution in the CH_3^+ TOF spectrum to methyl radicals from a primary S–CH_3 bond photofission channel in CH_3SO_2Cl at 193 nm. Indeed, using the higher kinetic energy portion of the speed distribution of the methyl radicals detected in the imaging experiments—and assuming that they resulted from primary S–CH_3 bond photofission in CH_3SO_2Cl at 193 nm—a very good fit to the TOF spectrum is obtained; it is shown in the lower frame in Fig. 6. The corresponding total recoil kinetic energy distribution for this primary S–CH_3 bond photofission channel is shown in Fig. 10. We did attempt to look for products from the momentum-matched $m/e=99$ (SO_2Cl) cofragment in other TOF spectra, noting that the SO_2Cl cofragment dissociates easily (low energetic barrier) to SO_2+Cl, probably with little additional kinetic energy release; the resulting cofragment is so heavy that the predicted arrival times would closely overlap the contribution from clusters in the Cl^+ and SO_2^+ TOF spectra, so cannot be confirmed. Those fits are shown in the EPAPS supplement.

To estimate a rough branching ratio between this S–CH_3 photofission channel and the S–Cl photofission channel that produces CH_3SO_2 radicals, we took 14 spectra at each of $m/e=15$ and $m/e=35$. Each spectrum was accumulated for 250 000 laser shots to give a total of 3.5×10^6 shots at each mass, alternating between the respective masses to average out drifts in beam intensity, etc. We then integrated the relevant components in each spectrum (channels 50–100 for the $m/e=35$ spectrum and channels 40–65 for the $m/e=15$ spectrum) to account for the fraction of the signal from the fits in Fig. 2 and the lower frame of Fig. 6. To arrive at a rough determination of the branching ratio between S–CH_3 photofission and S–Cl photofission, the integrated signal is then corrected for the ^{35}Cl isotope fraction $f_{^{35}Cl}$, the expected signal sensitivity due to differing kinematics and Jacobian factors (including transit time through the ionizer), the electron bombardment ionization cross sections σ_{ion}, and the daughter ion fragmentation pattern of methyl radicals f_{CH3/CH_3^+}. We obtain

$$\frac{\sigma_{S-CH_3}}{\sigma_{S-Cl}} = \left(\frac{\text{integrated signal at } CH_3^+}{\text{integrated signal at } {}^{35}Cl^+}\right)(f_{^{35}Cl})\left(\frac{\text{expected signal with Cl kinematics}}{\text{expected signal with } CH_3 \text{ kinematics}}\right)\left(\frac{\sigma_{ion,Cl}}{\sigma_{ion,CH_3}}\right)\left(\frac{f_{Cl^+/Cl}}{f_{CH_3^+/CH_3}}\right)$$

$$= \frac{\sigma_{S-CH_3}}{\sigma_{S-Cl}} = \left(\frac{17\,947}{198\,219}\right)(0.7578)\left(\frac{0.0816}{0.0503}\right)\left(\frac{35.2}{51.8}\right)\left(\frac{1}{0.5}\right) = 0.26. \quad (2)$$

The electron bombardment cross sections are estimated roughly from the empirical formula proposed by Center and Mandl,[19] with the sum of atomic polarizabilities calculated from those of Miller and Bederson.[20] This estimate is not expected to be better than ±20%. The daughter ion cracking pattern of methyl radicals changes gradually with internal energy and has been measured for 70 eV electron bombardment; we use the low internal energy value of 0.5 for the signal at $m/e=15$, divided by the sum of the signals at $m/e=15$, 14, 13, and 12 as determined by Lin in his unpublished data[21] from methyl iodide photodissociation at 157 nm. As $S-CH_3$ and S–Cl fission are the only two primary photodissociation channels detected, we thus estimate that $S-CH_3$ fission accounts for 20% of the photofragment yield while S–Cl fission accounts for 80% of the photofragment yield.

F. Photofragment angular distribution data

To determine the angular distribution of the Cl fragments, we integrate the TOF spectra taken at each of the seven laser polarization angles. Because our experimental data evidenced the formation of both ground and electronically excited-state CH_3SO_2 radicals, we integrate the signal corresponding to the high kinetic energy S–Cl bond fission channel and the signal corresponding to the lower kinetic energy S–Cl bond fission channel separately. Signal appearing from the high kinetic energy channel, identified above as the ground-state product channel, is integrated from 110 to 150 μs. The signal from the low kinetic energy channel, the excited-state product channel, is integrated from 152 to 350 μs. To determine the anisotropy parameter β from the integrated intensities, we begin with the classical electrical dipole expression [Eq. (3)],

$$I(\theta_{cm}) = \frac{1}{4\pi}[1 + \beta P_2(\cos(\theta_{cm}))]. \quad (3)$$

In this equation, θ_{cm} is the angle between the electric vector of the linearly polarized light and the fragments' recoil direction in the center-of-mass reference frame and P_2 is the second-order Legendre polynomial. We then use the standard forward convolution procedure to predict the variation in signal intensity expected for each of the two components in the TOF spectra, integrated over the ranges given, as the angle of polarization is changed. The anisotropy parameter is varied to obtain a good fit to the integrated data. For the high kinetic energy S–Cl fission channel, our data are best fitted by an anisotropy parameter of $\beta=0.56$ with the 95% confidence interval ranging from $\beta=0.47$ to $\beta=0.65$, as shown in Fig. 11. The signal from the low kinetic energy S–Cl bond fission channel, Fig. 12, was best fitted by an anisotropy parameter of $\beta=0.8$. Figure S.11 in the EPAPS supplement shows the individual fits for the TOF spectra obtained at each of the seven laser polarization angles.

IV. DISCUSSION

This study resolved the differences between the dissociation dynamics of vibrationally excited ground state CH_3SO_2 radicals and electronically excited-state $(1\,^2A'', 2\,^2A'')$ CH_3SO_2 radicals formed from the photodissociation of CH_3SO_2Cl. The ground state radicals dissociated to $CH_3 + SO_2$ via a loose transition state. The measured distribution of recoil kinetic energies in this dissociation shows that the molecule does not experience significant repulsive forces along the C–S bond after the transition state. This is consistent with the electronic structure results presented in the preceding paper, which show no barrier beyond the endoergic-

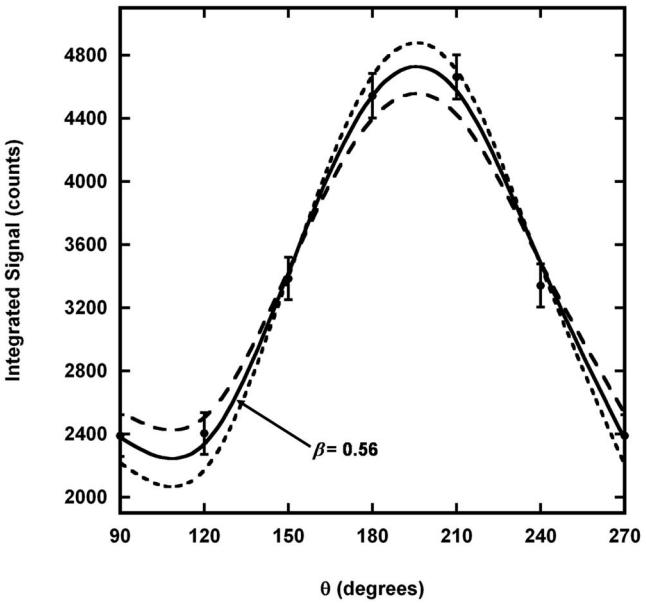

FIG. 11. Angular distribution of the Cl fragments formed in the high-recoil kinetic energy channel following photodissociation of methylsulfonyl chloride. The portion of the Cl signal integrated from 110 to 150 μs is plotted as a function of the angle between the electric vector of the laser and the line from the interaction region to the detector. The integration range corresponds to the fast peak in each TOF distribution (see Fig. 2). The experimental data (solid circles) are shown with ±σ error bars. The best fit is calculated from an anisotropy parameter $\beta=0.56$ (solid line). The short and long-dashed lines show the fits calculated from the upper and lower limits, respectively, of the 95% confidence interval for β.

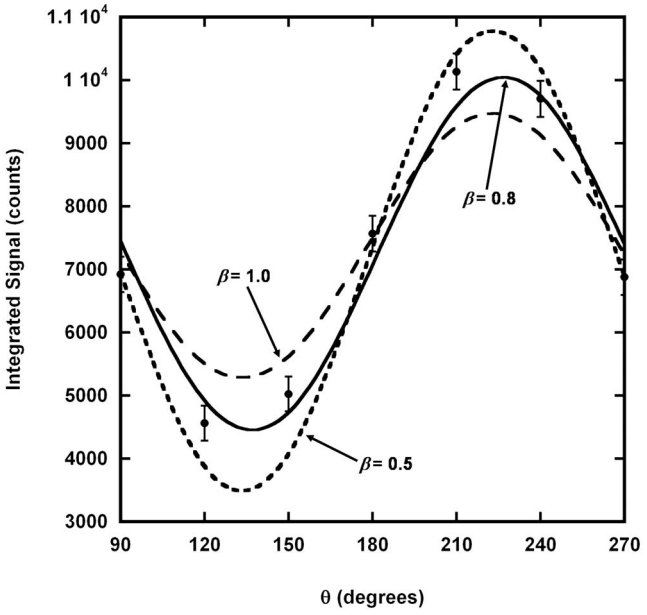

FIG. 12. Angular distribution of the Cl fragments formed in the low recoil kinetic energy channel following photodissociation of methylsulfonyl chloride. The portion of the Cl signal integrated from 152 to 350 μs is plotted as a function of the angle between the electric vector of the laser and the line from the interaction region to the detector. The integration range corresponds to the slow peak in each TOF distribution (see Fig. 2). The experimental data (solid circles) are shown with $\pm\sigma$ error bars. The best fit is calculated from an anisotropy parameter β=0.8 (solid line). The short- and long-dashed lines show the fits calculated from an anisotropy parameter of β=0.5 and β=1.0, respectively.

ity. Indeed, our data are quite well fitted by a statistical prediction of this kinetic energy distribution from the CCSD(T) computed transition state assuming no redistribution of energy after the transition state. Interestingly, the other radical isomer, CH_3OSO (not studied here), is predicted to have a substantial barrier beyond the endoergicity, by about 12 kcal/mol, to dissociate to CH_3+SO_2. We hope to resolve those dynamics in future studies.

In contrast to the ground state dissociation dynamics, the dissociation dynamics of electronically excited ($1\ ^2A'', 2\ ^2A''$) CH_3SO_2 radicals to CH_3+SO_2 partitions substantial energy into recoil translational energy; this indicates that the dissociating molecule encounters repulsive forces in the C–S coordinate outside of the Franck–Condon region. Therefore, the data show that dissociation of excited-state radicals does not proceed via internal conversion to the ground electronic state, but rather via an electronic predissociation. This is important in reinterpreting the prior experimental results of Baronavski and co-workers as discussed below. Our CCSD(T) calculations also predict the energetics of these excited states for comparison with the present results, as well as the results of prior studies of these excited states. The UV absorption spectrum of methylsulfonyl radicals has not been measured in the gas phase, but has been measured in solution. The most recent study was in an isooctane solution by Chatgilialoglu *et al.*;[22] that paper also reports theoretical calculations to predict the vertical transition energies and the oscillator strengths for the transitions. Their measured UV absorption is broad and structureless with a maximum at 350 nm. They assign the absorption to transitions involving the $1\ ^2A''$, $2\ ^2A''$, and $2\ ^2A'$ states of CH_3SO_2 radicals; the calculated vertical transitions to these states are reported as 370, 330, and 320 nm, respectively, with calculated oscillator strengths of 0.045, 0.629, and 0.207. That work does not report any calculations of adiabatic excitation energies. Our CCSD(T) calculations predict that the adiabatic excitation energy to the lowest excited state of CH_3SO_2, the $1\ ^2A''$ state, is substantially lower than the vertical excitation energy. The calculated adiabatic excitation energy of 34.8 kcal/mol gives an energetic limit to the formation of excited-state CH_3SO_2 from the photodissociation of CH_3SO_2Cl at 193 nm. The primary S–Cl bond fission must partition less than 50 kcal/mol to recoil kinetic energy in order to leave the nascent CH_3SO_2 radical with enough internal energy for it to access the $1\ ^2A''$ excited state. In agreement with this calculated limit, all of the signal from the slower portion of the recoil kinetic energy S–Cl bond fission distribution, shown by the short-dashed line in Fig. 3, partitions less than 50 kcal/mol to product translation; we assign this portion of the overall distribution to the $Cl+CH_3SO_2$ ($1\ ^2A'', 2\ ^2A''$) channel. The predicted vertical transition energies of these two A'' states and the $1\ ^2A'$ state are much higher than the adiabatic excitation energy and are in good agreement with the prior calculations.

This paper also presents calculations of the critical points on the ground electronic state potential energy surface with the G3//B3LYP method. Because the G3//B3LYP results are substantially less computationally expensive than those obtained with the CCSD(T) method, one may prefer to use the fairly reliable G3//B3LYP method for molecular systems where the CCSD(T) method is infeasible. As found in this study, the G3//B3LYP results give minima and transition states having energetics within 2.5 kcal/mol of the CCSD(T) results for all the structures studied in this work and within one kcal/mol of the CCSD(T) prediction for the dissociation barrier measured in the experiments. Some of the Zhu and Bozzelli results could be erroneous because of the inadequate size of the basis sets that were used on the sulfur-containing compounds. The choice of basis sets for these sulfur-containing radicals is most important; even somewhat larger basis sets do not yield the required chemical accuracy. As an example, the dissociation barrier to CH_3+SO_2 is calculated to be only 12.8 kcal/mol at the CCSD(T)/6-311++G($2df,p$)+ZPVE level of theory. Guided by the CCSD(T) predicted dissociation barrier of 14.6 kcal/mol, we obtain a good fit for the expected velocity distribution of those surviving CH_3SO_2 radicals (detected at its m/e=15 CH_3^+ daughter ion) and the sharp high-recoil velocity distribution observed in the actual TOF spectrum for the m/e=15 ion. This indirectly supports the reliability of the current CCSD(T) predicted dissociation barrier, which has been done with quadruple-zeta basis sets and incorporating essential relativistic and core-valence corrections for the sulfur-containing compounds.

The computational work here also analyzes the surprising differences between the predicted isomerization barriers for $CH_3SO_2 \rightarrow CH_3OSO$ reported in two prior studies. We redid the calculations of this isomerization reported by Frank and Turecek at their same level of theory and found that they had misidentified the transition state structure. More impor-

tantly, our G3//B3LYP and CCSD(T) results for this isomerization barrier are in reasonable agreement. The G3//B3LYP method includes a semiempirical correction, which was determined by minimizing the average absolute deviation from experiment for a test set with 299 energies; the test set does not contain any data pertaining to transition state barriers. Nevertheless, it is encouraging to see that the current G3//B3LYP prediction for the isomerization barrier comes very close to the CCSD(T) prediction.

This work also allowed us to identify another primary photodissociation channel of CH_3SO_2Cl at 193 nm, that of $S-CH_3$ bond fission. Identifying this channel with our methodology is problematic because the cofragment of CH_3 in this channel, SO_2Cl, is energetically unstable, dissociating to SO_2+Cl. The measurement of SO_2, CH_3, and Cl atom velocity distributions—along with that of the stable CH_3SO_2 radicals—allowed us to definitively show that not all of the methyl radical products result from photofission of the Cl bond followed by dissociation of the CH_3SO_2 cofragment. While the slower methyl radicals were momentum matched to the SO_2 products from the unimolecular dissociation of CH_3SO_2, the highest velocity CH_3 products result from a process where the $S-CH_3$ bond in CH_3SO_2Cl breaks photolytically. The dotted gray line fit in the upper frame of Fig. 6 shows that the speed distribution of the methyl radicals detected in the $m/e=15$ spectrum here is in good agreement with the speed distribution of methyl radicals detected in the imaging experiments in the preceding paper, as must be the case if photoionization at 10.5 eV does not favor the detection of some methyl radicals over others.

Finally, this work suggests that the prior results of Baronavski and co-workers, which attempted to use time-resolved photoionization to probe the unimolecular dissociation of CH_3SO_2 radicals, need reinterpretation. They did not consider the possibility that their photolytic precursor formed a substantial fraction of CH_3SO_2 radicals in an electronically excited state. The fact that it does compromises two portions of their analysis. First, note that the energy of the two 259 nm (4.8eV) photons used in their ionization process is below the calculated CH_3SO_2 vertical ionization energy of 9.72 eV, calculated using the G3X method.[23] If their two-photon photoionization was preferentially sensitive to detecting electronically excited radicals, it could explain the reason for their signal decaying to near baseline in 2 ps. Additionally, our measured internal energy distribution for the ground state radicals includes a substantial fraction of radicals near and below the dissociation barrier, which is inconsistent with their interpretation of the time-resolved data. Their results might still provide useful data on the dissociation dynamics of ground-state radicals if the nascent electronically excited radicals dissociated via fast internal conversion to the ground state potential energy surface, followed by slow secondary dissociation on the ground state potential. However, our data also show that the electronically excited radicals do not dissociate via internal conversion to the ground state potential energy surface; the partitioning to recoil kinetic energy in the dissociation of the electronically excited radicals is too large. Thus, their interpretation of the time-resolved data based on rate calculations on the ground state potential energy surface is in error. Using a higher photon energy for photoionization in such time-resolved experiments could, however, yield key results. Our experimentally determined internal energy distributions show that, if the higher photon energy allowed one to efficiently ionize the ground state radicals produced in our high-recoil kinetic energy S–Cl photofission channel, such data would be quite sensitive to the microcanonical unimolecular dissociation rate spanning energies important for thermal predictions. We include some relevant predictions for such experiments in the preceding paper.

ACKNOWLEDGMENTS

The experimental work herein was supported by the National Science Foundation (Grant No. CHE-0746050, L.J.B.) and the Donors of the American Chemical Society Petroleum Research Fund (Grant No. 47480-AC6, L.J.B.). The CCSD(T) and EOMEE-CCSD computational results presented here were supported by a grant from the Research Grants Council of the Hong Kong Special Administrative Region, China (Project No. CityU 101507, K.C.L.). One of the authors, E.J.G., acknowledges the financial support of the Arnold and Mabel Beckman Foundation.

[1] M. Speidel, R. Nau, F. Arnold, H. Schlager, and A. Stohl, Atmos. Environ. **41**, 2427 (2007).
[2] A. Saltelli and J. Hjorth, J. Atmos. Chem. **21**, 187 (1995).
[3] S. B. Barone, A. A. Turnipseed, and A. R. Ravishankara, Faraday Discuss. **100**, 39 (1995).
[4] A. J. Frank and F. Turecek, J. Phys. Chem. A **103**, 5348 (1999).
[5] L. Zhu and J. W. Bozzelli, J. Mol. Struct.: THEOCHEM **728**, 147 (2005).
[6] J. C. Owrutsky, H. H. Nelson, and A. P. Baronavski, J. Phys. Chem. A **105**, 1440 (2001).
[7] B. J. Ratliff, X. N. Tang, L. J. Butler, D. E. Szpunar, and K. -C. Lau, **131**, 044304 (2009).
[8] J. M. L. Martin, J. Chem. Phys. **108**, 2791 (1998).
[9] D. Borissenko, A. Kukui, G. Laverdet, and G. Le Bras, J. Phys. Chem. A **107**, 1155 (2003).
[10] A. Ray, I. Vassalli, G. Laverdet, and G. Le Bras, J. Phys. Chem. **100**, 8895 (1996), and earlier references within.
[11] A. Kukui, V. Bossoutrot, G. Laverdet, and G. Le Bras, J. Phys. Chem. A **104**, 935 (2000).
[12] Y. T. Lee, J. D. McDonald, P. R. LeBreton, and D. R. Herschbach, Rev. Sci. Instrum. **40**, 1402 (1969).
[13] N. R. Daly, Rev. Sci. Instrum. **31**, 264 (1960).
[14] See EPAPS supplementary material at http://dx.doi.org/10.1063/1.3159555 for energies, geometries, and moments of inertia of the intermediates and transition states for the CH_3SO_2 potential energy surface, calculated at the G3//B3LYP level of theory, along with supplemental experimental data. The second supplementary file gives the optimized geometry of the lowest doublet excited state of CH_3SO_2 calculated at the CCSD(T) level of theory described herein.
[15] A. G. Baboul, L. A. Curtiss, P. C. Redfern, and K. Raghavachari, J. Chem. Phys. **110**, 7650 (1999).
[16] M. J. Frisch, G. W. Trucks, H. B. Schlegel *et al.*, GAUSSIAN03, Revision C.02 Gaussian, Inc., Pittsburgh, PA, 2003.
[17] J. F. Stanton, J. Gauss, J. D. Watts, P. G. Szalay, and R. J. Bartlett, with contributions from A. A. Auer, D. E. Bernholdt, O. Christiansen, M. E. Harding, M. Heckert, O. Heun, C. Huber, D. Jonsson, J. Jusélius, W. J. Lauderdale, T. Metzroth, C. Michauk, D. P. O'Neill, D. R. Price, K. Ruud, F. Schiffmann, M. E. Varner, J. Vázquez and the integral packages

by J. Almlöf and P. R. Taylor, MOLECULE, P. R. Taylor, PROPS, and T. Helgaker, H. J. Aa. Jensen, P. Jørgensen, and J. Olsen, ABACUS. For the current version, see http://www.aces2.de.
[18] H.-J. Werner, P. J. Knowles, R. Lindh *et al.*, MOLPRO, version 2006.1, a package of *ab initio* programs, see http://www.molpro.net.
[19] R. E. Center and A. Mandl, J. Chem. Phys. **57**, 4104 (1972).
[20] T. M. Miller and B. Bederson, Adv. At. Mol. Phys. **13**, 1 (1977).
[21] J. J. Lin, private communication, 2001. Daughter fragmentation pattern of methyl radicals upon 70 eV electron bombardment detection from the photodissociation of CH3I at 157 nm, dispersing the methyl radicals as a function of internal energy from 3 to 88 kcal/mol in 5 kcal/mol increments.
[22] C. Chatgilialoglu, D. Griller, and M. Guerra, J. Phys. Chem. **91**, 3747 (1987).
[23] L. A. Curtiss, P. C. Redfern, K. Raghavachari, and J. A. Pople, J. Chem. Phys. **114**, 108 (2001).